Water Research 271 (2025) 122856

Contents lists available at ScienceDirect

Water Research

journal homepage: www.elsevier.com/locate/watres

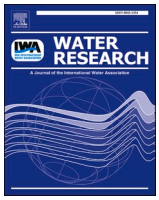

Impact of particle size and oxide phase on microplastic transport through iron oxide-coated sand

Yongjoon Choe [a], Jongmuk Won [b,*], Susan E. Burns [a]

[a] School of Civil and Environmental Engineering, Georgia Institute of Technology, 790 Atlantic Drive, N. W., Atlanta, GA, 30332-0355, Georgia
[b] Department of Civil, Urban, Earth, and Environmental Engineering, Ulsan National Institute of Science and Technology (UNIST), UNIST-gil 50, Ulju-gun, Ulsan 44919, Republic of Korea

ARTICLE INFO

Keywords:
Polystyrene microplastic
Iron oxide-coated sand
Hematite
Goethite
Magnetite
Column experiment

ABSTRACT

The presence of microplastics in aquatic environments threatens the ecological system and human health. This study investigates the transport and retention of polystyrene microplastics (PSMPs) in clean sand, and hematite-, goethite-, and magnetite-coated iron oxide - sands as a function of size ratio and ionic strength. The breakthrough curves (BTCs), retention profiles, and hydraulic pressure were measured through soil-column experiments, and the retention of PSMPs was assessed from the observed BTCs, RPs and first-order attachment coefficients. In addition, the maximum attachment capacity was evaluated to assess the long-term retention of PSMPs. Experimental data showed that the retention of PSMPs increased in the order of goethite-, hematite-, and magnetite-coated sands in all size ratios, which is consistent with the order of attraction energy calculated by extended Derjaguin-Landau-Verwey-Overbeek theory. The findings demonstrated the feasibility of mitigating the transport of microplastic particles using naturally abundant iron-rich soils.

1. Introduction

The yearly production of plastic (currently at 430 million tons) is expected to triple over the next 25 years (Ritchie et al., 2023). However, improper management of plastic waste that is not recycled, incinerated, or contained in landfills can potentially introduce plastics into marine and terrestrial environments, leading to environmental pollution (Geyer et al., 2017; Kibria et al., 2023). Those plastic wastes are weathered or degraded into microplastics (MPs) with particle sizes ranging from 0.1 μm –5 mm by mechanical, chemical, and biological processes (Alimi et al., 2022; Blaga, 1980; Büks and Kaupenjohann, 2022; Cooper, 2012; Corcoran, 2022; Duan et al., 2021; Liu et al., 2020; Song et al., 2017). Due to their small particle sizes, MPs can be transported to the marine (Andrady, 2011), coastal (Carpenter et al., 1972), and soil environments (Boots et al., 2019; Li et al., 2020; Shruti et al., 2021) by runoff, wind, or plants and animals (Auta et al., 2017; Ebere et al., 2019; Hitchcock, 2020). As plastics production has increased, MPs are more frequently found in natural environments, which eventually leads to a increased health risks such as obesity, oxidative stress, and decreased growth rate (Deng et al., 2017; Jeong et al., 2024; Karbalaei et al., 2018). Because MPs can be transported through single or multiple environmental compartments, previous research investigated the transport behavior of MPs through various environmental compartments (Horton and Dixon, 2018). Due to its toxicity and challenging transport behavior, understanding the transport of MPs has been one of the critical research topics in environmental engineering.

Plastic particles typically have surface charge with an isoelectric point (IEP) that is either slightly acidic or neutral pH with a negative charge in most natural aquatic environments (Fotopoulou and Karapanagioti, 2012). Furthermore, the aging process enhances the functionality of the MP surface, thereby increasing both its wettability and electronegativity (Al Harraq and Bharti, 2022; Brewer et al., 2020). As a result, MPs interact with charged substances in the soil, such as clay minerals, heavy metals, or organic materials. These interactions influence the fate and distribution of MPs within the soil (Chang et al., 2023; Selvam et al., 2021; Wang et al., 2021). In iron-rich terrestrial environments, MPs can be transported along with seepage and interact with iron oxides, either in their colloidal state or attached to soil particles. When both MPs and iron oxides are in a colloidal state, the iron oxides reduce the repulsive forces around the MPs, facilitating the co-aggregation of iron oxides and MPs (Vu et al., 2022). When iron oxides were attached to sand particle surfaces, it reduced the energy barrier of sand particles by increasing surface charge heterogeneity (Chen et al., 2019), which enhances the complexity of interaction energy

* Corresponding author.
E-mail addresses: ychoe31@gatech.edu (Y. Choe), jwon@unist.ac.kr (J. Won), susan.burns@ce.gatech.edu (S.E. Burns).

https://doi.org/10.1016/j.watres.2024.122856
Received 13 August 2024; Received in revised form 8 November 2024; Accepted 25 November 2024
Available online 28 November 2024

due to increased nanoscale surface roughness (Bradford et al., 2017; Dong et al., 2024). In addition, the presence of chemically bonded iron oxides on the surfaces of sand can increase the coordination number (Larrahondo et al., 2011). Therefore, the transport of MPs through sand with iron oxides can be influenced by interaction energy between MPs and iron oxides and the unique geometrical effects of iron oxide-attached sand.

Despite the prevalence of iron oxides in natural environments, the transport of MPs through iron oxide-attached sand has not been well understood. The iron oxide-attached sand can be simulated as iron oxide coated sand (IOCS) in laboratory-scale experiments (Chang et al., 2023; Larrahondo and Burns, 2014), which has been reported as one of the low-cost promising mediums for removing nano-sized particles including bacteria (Ahammed and Davra, 2011), arsenic (Joshi and Chaudhuri, 1996; Thirunavukkarasu et al., 2003), ammonia-complexed cationic metals (Cu, Cd, Pb, Ni, Zn), oxy anionic metals (SeO_3, AsO_3) (Benjamin et al., 1996; Stahl and James, 1991). Recently, transport and retention of polystyrene MPs (PSMPs) using IOCS has been studied under electrolyte solutions (IS > 1 mM) and various pH ranges with size ratio (SR; d_{sand}/d_{PSMP}) higher than 1000 (Chang et al., 2023; Wu et al., 2022). However, the fundamental transport behavior of PSMP through IOCSs, particularly under a relatively low SR and dilute solution (high repulsion) has not been well documented.

Therefore, this study aims to investigate PSMP transport through three types of laboratory-prepared IOCSs (hematite-, goethite-, and magnetite-coated sands) using a series of soil column experiments. Negatively charged PSMP (particle size of 1 μm) was selected to simulate microplastic transport through soils because the relatively small particle size has been reported to be harmful to human health (Hwang et al., 2020) and unfavorable attachment conditions (negatively charged colloidal particles and collectors) are prevalent in the geochemical conditions of subsurface environments. The impact of ionic strength (IS) and the type of iron oxide on the transport or retention of PSMP were investigated through the observed retention profiles (RPs) and breakthrough curves (BTCs). In addition, an extended Derjaguin-Landau-Verwey-Overbeek (XDLVO) approach was applied to quantitatively calculate the interaction energy between IOCS and PSMPs to discuss the observed results. Implications of observed results on PSMP transport through iron-rich soils are also discussed.

2. Materials and methods

2.1. Materials

In this study, sands with median grain sizes (d_{50}) of 120 μm, 360 μm, 550 μm, and 720 μm were used in the experiments (specific gravity (G_s) = 2.65; coefficient of uniformity < 1.3). For IOCS, three types of iron oxides were utilized: hematite (α-Fe_2O_3), goethite (α-FeOOH), and magnetite (Fe_3O_4). The X-ray diffraction (XRD) and X-ray fluorescence analysis (XRF) confirmed that the clean sand and iron oxides showed specific peaks for quartz, hematite, goethite, and magnetite (Fig. S1 and Table S1 in Supplementary Information). To prepare IOCS, the heterogeneous suspension reaction method was selected to enable stable and strong attachment of iron oxide particles to the sand surface in pH 4 – 9 without release of iron ions (Hanna, 2007; Lai et al., 1994; Larrahondo et al., 2011). The preparation process of IOCS is as follows: silica sand was placed on a #200 sieve (opening size of 0.074 mm) and washed with deionized (DI) water several times to remove impurities. Next, the sand

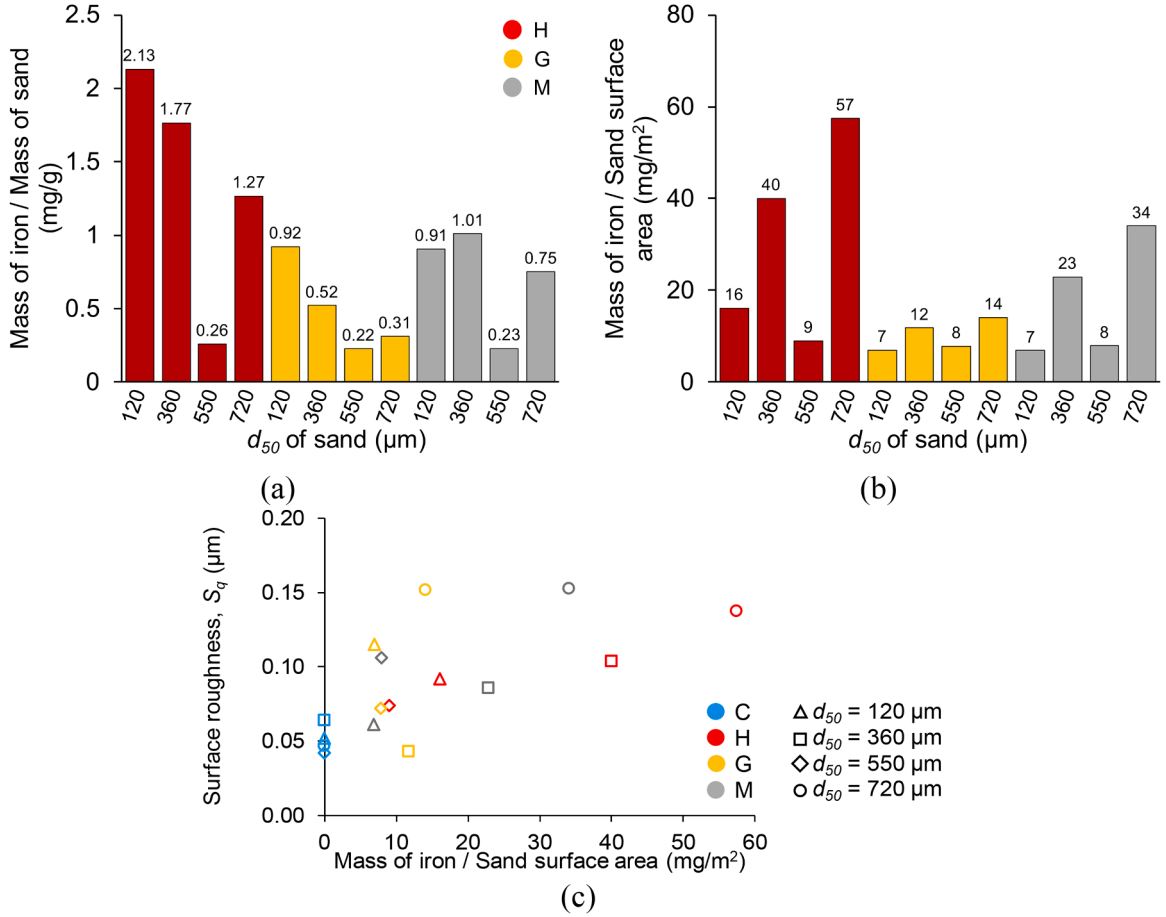

Fig. 1. Mass of iron per unit mass of sand ((a)), mass of iron per unit sand surface ((b)), and surface roughness (S_q in Table S2) as a function of mass of iron per unit sand surface ((c)). Note: *C* = clean sand; *H* = hematite coated sand; *G* = goethite coated sand; *M* = magnetite coated sand.

was washed with 3 % H_2O_2 solution followed by a DI water rinse to remove organic matter, and oven-drying at 100 °C for 24 h. After drying, 1 g of sand and 40 mg of iron oxide powder were combined with 1000 mL of DI water and mixed using a rotary mixer for 24 h. The suspension was filtered to separate IOCS before washing 10 times to remove any loosely attached iron oxide particles. The IOCS was oven-dried at 100 °C for 24 h to obtain stable IOCS.

After preparing IOCS, the iron oxide content of IOCS (Fig. 1) was determined by desorbing the iron oxides from the IOCS using the dithionite-citrate-bicarbonate technique, followed by measuring the iron concentration using Inductively Coupled Plasma-Optical Emission Spectrometry (ICP-OES). In addition, the surface roughness of clean sand and IOCSs was characterized by randomly selecting an area of 16 μm × 16 μm on the surface of the sand using laser microscopy (OLS5100). As seen in Table S2, the surface roughness parameters of IOCSs were higher (rougher) than clean sand, as anticipated. In addition, as the d_{50} of the tested particles increased, the adsorbed mass of iron per unit mass of sand decreased (Fig. 1(a)); however, iron mass sorbed increased per unit surface area of tested sand (Fig. 1(b)) (with the exception of d_{50} = 550 μm). Note that the low iron content of 550 μm sand shown in Fig. 1(a) can be attributed to the higher roundness and lower roughness of 550 μm sand than other three types of sand, which leads to the low coating efficiency of 550 μm sand (Fig. S2 and Table S2).

Carboxylate-modified polystyrene latex microspheres with 1 μm diameter (Sigma-Aldrich) were used as negatively charged PSMPs (G_s = 1.055). The concentration of stock suspension was 40 g/L, which was diluted to the concentration of 7.5 mg/L in the column experiments. The PSMP concentration of 7.5 mg / L was selected to simulate aquatic environments, which is consistent with the range of microplastic concentration (1 to 30 mg/L) used in the literature (Cai et al., 2016; Hoggan et al., 2016; Magal et al., 2011; Mitropoulou et al., 2013). The zeta potentials of IOCS and PSMPs were measured using a zeta potential analyzer (Malvern Zetasizer) where the pretreatment method for IOCS in literature (Chang et al., 2023; Dong et al., 2024) was selected in this study. Specifically, 10 g of IOCS were mixed with 40 mL of background electrolyte solution and sonicated for 30 min before measuring the zeta potential of the suspension, which is regarded as the equivalent zeta potential of IOCS. Pictures and the images from Laser Confocal Scanning Microscopy of clean sands and IOCSs used in this study are presented in Figs. S2, S3 and S4 respectively.

2.2. Experimental design and analytical method

An acrylic column with height and diameter of 76.2 and 25.4 mm, respectively, was designed for the column experiments (Fig. S5). The saturated clean sand or IOCS column was prepared using the wet pluviation method. Assuming that e_{min} and e_{max} values of IOCS were equivalent to clean sand (Table S2), the sand column was prepared at relative density of 75 % (dense state) (corresponding to porosity of 0.359, 0.364, 0.364, and 0.387 for SR = 720, 550, 360, and 120) to prevent any change in pore structure during the injection. The fully saturated state was confirmed by measuring the weight of water in the column after preparing the saturated sand medium (Choe et al., 2022; Won et al., 2023). To investigate the breakthrough and tailing behavior of PSMP transport, 7.5 mg/L of the PSMP suspension was injected at the top of the column during the first 5 pore volumes (PVs) of flow, followed by injection with background solution for 5 PVs. The PSMP concentration of 7.5 mg / L was selected to simulate aquatic environments, which is consistent with the range of microplastic concentration (1 to 30 mg/L) used in the literature (Cai et al., 2016; Hoggan et al., 2016; Magal et al., 2011; Mitropoulou et al., 2013; Peng et al., 2017; Torkzaban et al., 2008). A constant flow rate of 2 mL/min was applied during a total injected volume of 10 PVs. The pore fluid background solution was either DI water (IS ≈ 0) or water with IS = 5 mM and pH = 6.9, controlled by NaCl, HCl, and NaOH.

During the injection, the PSMP concentration at the outlet was measured using the Ultraviolet-Visible spectroscopy (Shimadzu UV-1800) at a wavelength of 515 nm (Fig. S6). The observed BTCs and RPs were modeled by the one-dimensional advection-dispersion-based mass balance equation to backcalculate the first-order attachment coefficient (k_{att}) and maximum attachment capacity (S_{max}) (Bradford et al., 2005, 2003). The XDLVO theory was employed to understand the interaction between PSMPs and IOCS under experimental conditions assuming a sphere (MP)-plate (IOCS) configuration. Detailed explanations for parameter optimization, XDLVO calculation, and optimized k_{att} and S_{max} are provided in the Supplementary Information (Fig. S7).

The mass of PSMP particles retained in the column was measured every 15.24 mm to evaluate RP of PSMP after injection. The sampled IOCS extracted from the column was mixed with known volume of water for ~ 5 min to induce the detachment of PSMP particles attached to IOCS surface. The measurement of PSMP concentration provided the mass of retained PSMP particles per unit mass of IOCS as a function of depth. From the observed BTC, the fraction of filtered PSMP (M_e) was calculated using the trapezoidal method and the fraction of retained PSMP (M_r) was calculated from the observed RP.

A differential pressure transducer with an operating range of 0–6.89 kPa (0–1 psi) with an accuracy of ± 0.25 % was installed between the inlet and the outlet to measure the hydraulic conductivity of sand medium during the injection. The hydraulic gradient of the column was evaluated from the measured pressure difference, which also enabled monitoring the reduction of hydraulic conductivity (i.e., increase in hydraulic gradient) caused by the retention of PSMP particles (Won et al., 2023; Won et al., 2020). From measured hydraulic conductivities, the average hydraulic shear stress (τ_{avg}) was calculated for the quantitative representation of hydrodynamic forces applied to PSMP particles. Detailed explanation for τ_{avg} calculation is provided in the Supplementary Information.

3. Experimental observations

3.1. Filtered PSMP particles

Increasing IS from ~0 M (DI water) to 5 mM resulted in lower PSMP breakthrough concentrations (i.e., higher attachment rate) for each sand particle size and type of iron oxide coating (Fig. 2). This implies the higher attraction energy between PSMP and sand (both clean sand and IOCS) at higher IS, which is consistent for other types of colloidal particles (Chang et al., 2023; Flury et al., 2004; Ren and Smith, 2013; Wikiniyadhanee et al., 2016; Yoshida and Suzuki, 2006), and resulted in a higher modeled k_{att} at IS = 5 mM compared to IS = 0 M for all sands tested (Figs. S8(a) and S8(b)).

Overall, the IOCS (hematite, goethite, and magnetite-coated sands) showed higher attachment of PSMP than clean sand, regardless of IS (Table S3). However, a more substantial attachment efficiency of IOCS compared to clean sand was observed at IS = 0 M (Figs. 2(a), 2(c), 2(e), and 2(g)) compared to IS = 5 mM (Figs. 2(b), 2(d), 2(f), and 2(i)), which is due to high attraction energy between clean sand and PSMP at IS = 5 mM. In other words, the retention of PSMP by IOCS is influenced by the electrostatic attraction energy between IOCS and PSMP, and when the IS of the pore fluid is high, the increase in attraction energy due to the presence of iron oxide and the resulting increase in retention of PSMP are not as significant as they are at low IS. In particular, the very low breakthrough concentrations for all sands shown in Fig. 2(b) implies that the impact of iron oxide on the retention of PSMP can be negligible at high IS and low d_{50} (SR < 120) of the sand medium. However, as SR increased, an increase in the breakthrough of PSMP for the three IOCS at d_{50} = 360 μm (Fig. 2(d)) indicates the presence of a threshold SR between 120 and 360 where the 100 % retention of PSMP becomes unfeasible.

The gradual increase in C/C_0 after breakthrough point for clean sand at IS = 0 M (Figs. 2(a), 2(c), 2(e), and 2(g); duplicated results were also provided in Fig S9 and Table S4) indicate that the decrease in

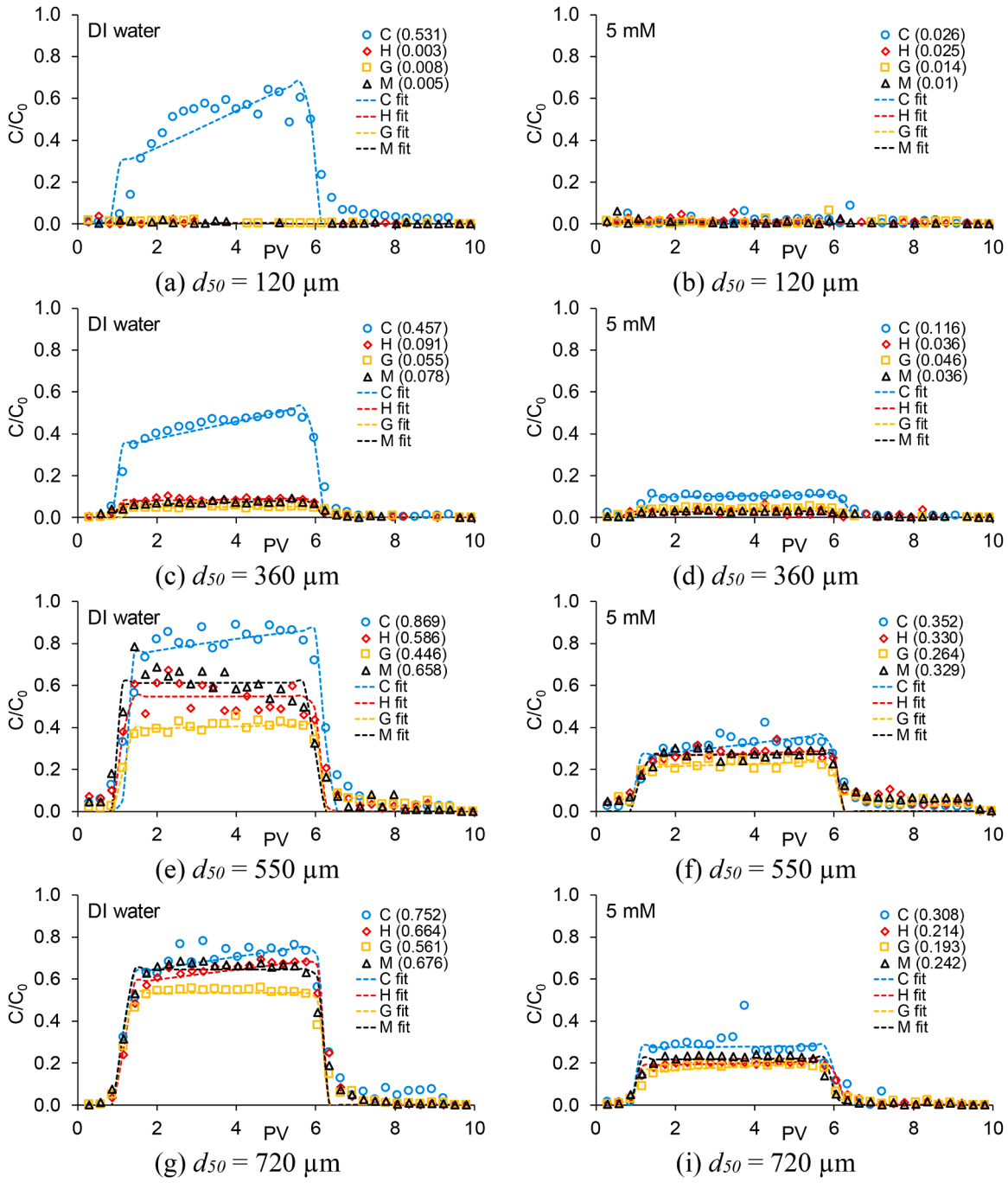

Fig. 2. Observed BTCs of PSMPs for all experimental conditions. The background solution consists of DI water ((a), (c), (e), and (g)) or a 5 mM NaCl solution ((b), (d), (f), and (i)) and d_{50} represents the median size of the sand particles. The numbers in parenthesis indicate the M_e (Table S1) in each case.

attachment rate caused by the decrease in available attachment sites at the surface of IOCS. This increasing trend confirms that the blocking mechanism (Eq. S3) may be valid to explain PSMP transport through the sand medium. It is notable that the retention of PSMP for clean sand was not significant, whereas almost 100 % retention was observed for the three IOCSs when d_{50} = 120 μm under DI water (Fig. 2(a)). Because the straining (retention of colloidal particle by pore size restriction) is not likely at SR > 125 (Bradford et al., 2005; Xu et al., 2006), attachment-dominant retention can be anticipated at the range of SR in this study (120 – 720). Thus, the higher retention of IOCS compared to clean sand (Figs. 2(a), 2(b), 2(e), and 2(g)) implies the higher attraction energy of IOC sands compared to clean sand for removing PSMPs. Nevertheless, C/C_0 between 0.4 and 0.6 in Figs. 2(a) and 2(c) indicate that a certain level of PSMP retention can be achieved using clean sand at low IS when sand particles are small (d_{50} is relatively low). Note that the higher C/C_0 observed at d_{50} = 550 μm compared to 720 μm in clean sand can be attributed to the higher hydraulic shear stress induced by the smaller pore size of 550 μm-sand. The calculated hydraulic shear stresses were 27.1 and 25.5 Pa for d_{50} = 550 μm and 19.0 and 21.7 Pa for d_{50} = 720 μm (Fig. S10). It can be also noted that the fluctuation of C/C_0 at SR = 550 (Figs. 2(e) and 2(f)) can be likely attributed to the surface charge heterogeneity of 550 μm sand because of relatively low iron content. This low iron content of 550 μm IOCS (Fig. 1(a)) can be attributed to the high roundness and low roughness of 550 μm sand (Figs. S2, S4, and Table S2), which decreases the coating efficiency.

Overall, higher breakthrough concentrations of PSMP was observed

in the IOCS when d_{50} increased. This can be attributed to the lower specific surface of the sand at higher d_{50}, which leads to the lower amount of iron oxides accessible to PSMPs at higher d_{50} (Fig. 1(a)). Therefore, it can be inferred that the higher amount of iron oxides in iron-rich sands can be beneficial in removing PSMPs. In addition, the impact of iron oxides on the retention of PSMPs becomes more significant at lower d_{50} as inferred from the substantial difference in C/C_0 between clean sand and the three IOCS at d_{50} = 120 and 360 μm. Note that the trend of observed BTCs as a function of d_{50} shown in Fig. 2 is consistent with the trend observed in literature for other types of colloidal particles such as clay (Chang et al., 2023; Saberinasr et al., 2016; Won and Burns, 2022).

The trend of modeled results (Fig. S8) was consistent with the observed BTCs in Fig. 2. Higher k_{att} at lower d_{50} (Figs. S8(a) and S8(b)) was obtained, which implies that the advection-dispersion-based model well described the transport of PSMPs through the sand medium. The higher k_{att} at IS = 5 mM than IS = 0 M is also consistent with the observed BTCs, indicating a higher attachment rate of PSMP can be anticipated at higher IS. Notably, even higher S_{max} at d_{50} = 120 μm than d_{50} = 360, 550 and 720 μm indicates that the relatively low particle size of sand enables the high long-term retention of PSMP at higher IS, particularly for sand with iron oxides. For example, the high S_{max} of H at d_{50} = 120 μm in Fig. S8(d) suggests highly available attachment sites of low d_{50} compared to high d_{50}. Note that the fitted k_{att} and S_{max} by observed RPs are also presented in Fig. S11 and Table S5, which showed similar trends as a function of SR and iron oxide type as those values based on the observed BTCs.

The gradual increase in C/C_0 after breakthrough point for clean sand at IS = 0 M (Figs. 2(a), 2(c), 2(e), and 2(g)) indicate that the decrease in attachment rate caused by the decrease in available attachment sites at the surface of IOCS. This increasing trend confirms that the blocking mechanism (Eq. S3) may be valid to explain PSMP transport through the sand medium. In addition, the difference in C/C_0 between DI water and IS = 5 mM at a given SR can be attributed to the more significant attraction energy between clean sand and PSMP particles compared to that between IOCS and PSMP particles. Because the IEP of clean sand (pH = 2–4) is even lower than that of the three iron oxides (pH = 7–8) (Choudhary et al., 2024; Cuddy et al., 2013; Rusch et al., 2010), the impact of IS on breakthrough PSMP concentrations is less significant for the three IOCSs than for clean sand, as observed in Fig. 2.

Comparing the three types of IOCS, the lowest breakthrough concentration was observed for goethite-coated sand (G), whereas the breakthrough concentration of hematite-coated sand (H) was slightly lower than magnetite-coated sand (M) for DI water ($G < H < M$) except for d_{50} = 360 μm ($M_e < 0.1$ for three IOCSs (Fig. 2(c))). The higher PSMP retention of G was particularly more pronounced at relatively high d_{50} of 550 and 720 μm at IS = 0 M ($G > H > M$ (d_{50} = 550 μm) or $G > H \sim M$ (d_{50} = 720 μm) (Figs. 2(e) and 2(g)). In contrast, the less significant difference in breakthrough concentration as a function of iron oxide type was observed for IS = 5 mM (Figs. 2(f) and 2(i)). Therefore, it can be suggested that goethite is the most efficient type of iron oxide in removing PSMPs, particularly under low IS. These results were consistent with the previous research (Rusch et al., 2010), which reported that G exhibits a higher attachment efficiency with PSMPs compared to H. The high attachment efficiency of G could be attributed to the higher surface area during the coating process with sand particles when compared to other iron oxides (Vu et al., 2022).

The abrupt decrease in C/C_0 at PV > 6 with almost no tailing effect indicates the stable attachment of PSMP particles on the sand medium without significant detachment. The slight fluctuation (e.g., d_{50} = 720 μm (Fig. 2(g)) or slight tailing effect (d_{50} = 120 μm (Fig. 2(a)) at IS = 0 M for clean sand indicates slight detachment of PSMP particles at the secondary minima because of relatively low attraction energy between PSMP and clean sand, as inferred from calculated interaction energy for IS = 5 mM (Fig. 3). The higher attraction energy of the three IOCSs compared to clean sand (Fig. 3) can support the higher retention and no tailing effect of the three IOCSs in the observed BTCs. Note that the attachment of PSMP particles likely occurs at the secondary minima (Shen et al., 2007).

The order of attraction energy between PSMPs and sand using XDLVO theory (Fig. 3(a)) is $G > M \sim H >$ clean sand, which was consistent with the observed BTCs (except for hematite / magnetite at IS = 0 M and d_{50} = 550 μm (Fig. 2(e))). However, the order of attraction energy as $H > G > M >$ clean sand was obtained when the Hamaker constant of hematite, magnetite, and goethite (Blakey and James, 2003; Faure et al., 2011) was applied for three IOCSs in XDLVO calculation (Fig. 3(b)). As the order of attraction energy after energy barrier for four types of sand is not qualitatively consistent with the observed BTCs, it can be inferred that the Hamaker constant for sand can be used in the qualitative assessment of PSMP transport through IOCSs.

3.2. Deposited PSMP particles

For IOCSs, the RP of PSMPs transitioned from a hyperexponential trend to a linear or log-linear trend with increasing d_{50} under both IS = 0 M and 5 mM (Fig. 4). The less exponential RPs for sands with higher d_{50} were consistent with the RPs of colloidal particles in previous studies (Albinger et al., 1994; Baygents et al., 1998; Bradford et al., 2011; Li et al., 2004; Redman et al., 2001) under unfavorable attachment conditions, characterized by a high energy barrier and weak interaction in the secondary minima (Fig. 3(a)). The less exponential RPs observed in almost all experimental conditions indicate almost no straining occurs at SR > 120 when PSMP particles were transported through clean sand and IOCS. In contrast, hyperexponential RPs (i.e., significant retention near

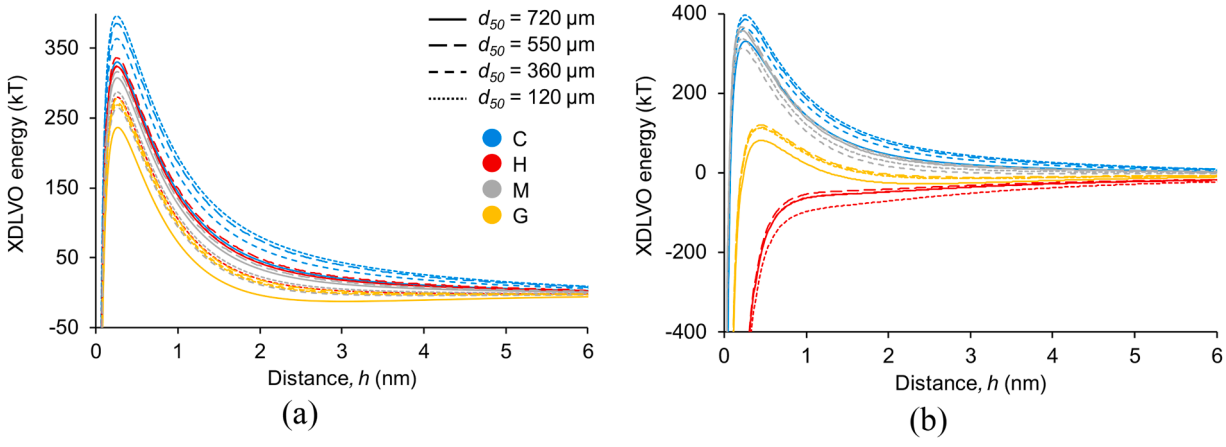

Fig. 3. The calculated interaction energy profiles between PSMP particle and clean sand ((a)) and PSMP particle and iron oxide particle ((b)) at IS = 5 mM.

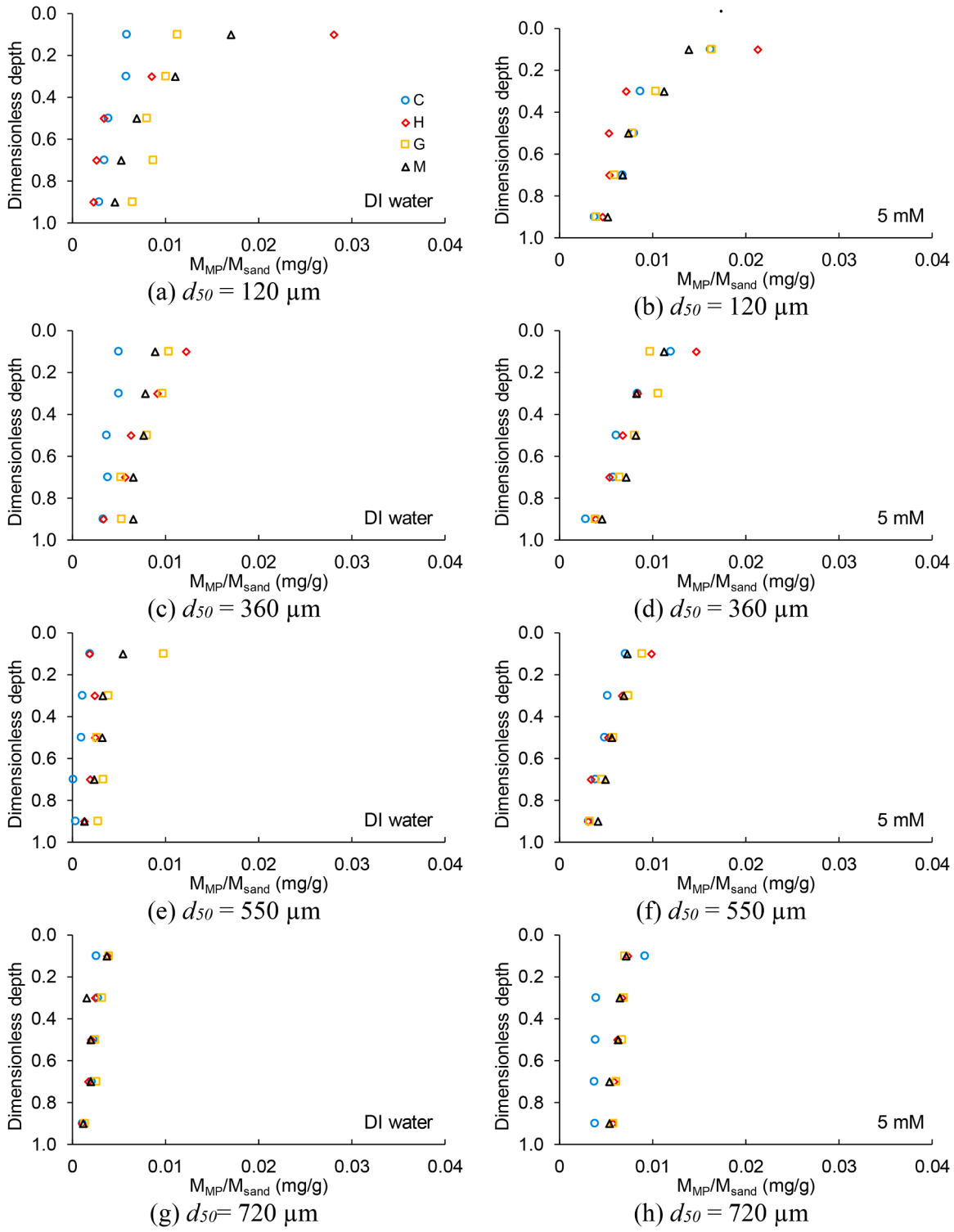

Fig. 4. Observed RPs of PSMPs. The background solution consists of DI water or a 5 mM NaCl solution, where d_{50} represents the median size of the sand particles.

the inlet) for H at SR = 120 (Figs. 4(a) and 4(b)) indicate a high chance of straining (Bradford et al., 2011; Wang et al., 2014), which indicates that significant retention of PSMPs at pore throat by size exclusion or bridging effect occurred. Because the attraction energy between *H* and PSMP particles calculated by XDLVO theory was comparable to that of *G* and *M*, the occurrence of straining for *H* can be attributed to its unique geometrical characteristics. The decrease in the size of the pore throat caused by coated iron oxide for H may be substantial compared to that for *G* and *M* because the hyperexponential RPs at SR = 120 were not observed for *G* and *M* (Figs. 4(a) and 4(b)).

The higher S_{max} for the three IOCS compared to clean sand implies that the more efficient long-term retention of PSMPs can be anticipated by the presence of iron oxides in sand surface (Fig. S8). For example, S_{max} = 0.143 mg/g for *G* at d_{50} = 550 μm (Fig. S8(c)) indicates that the long-term attachment capacity for *G* is 30 times higher than that for clean sand (S_{max} = 0.005 mg/g). The S_{max} = 1.207 mg/g (Table S3) and the maximum retained PSMP = 0.028 mg/g near the inlet for *H* at SR = 120 (Fig. 4(a)) implies highly available attachment sites after injecting 5

PVs of PSMP suspension. However, because S_{max} is only relevant to the attachment mechanism, the occurrence of straining for H at SR = 120 may clog the pore throats during long-term injection, which downgrades the long-term retention efficiency as the high fraction of H sorption sites far from the inlet may not be accessible. Apart from the cases of H at SR = 120 (high chance of straining), the high long-term retention of the three IOCSs can also be anticipated as S_{max} is higher than retained PSMP for SR = 120 and 360 (Fig. 4 and Fig. S8).

To assess the significant hyperexponential retention at SR = 120 for the hematite coating (Fig. 4(a)), additional experiments were performed using H with three low iron contents of 1.63 (HL1), 1.86 (HL2), and 2.34 (HL3) mg/m^2 (iron content of H = 16.07 mg/m^2) under IS = 0 M (Fig. 5 and Table S6). The almost linear RP for HL1, HL2, and HL3 (Fig. 5(a)) implies that the occurrence of hyperexponential retention in Fig. 4(a) for H can be attributed to the geometrical effect caused by the high hematite content. In addition, plateau concentration at the observed BTCs in order of HL1 > HL2 > HL3 shown in Fig. 5(b) implies that the retention of PSMP is sensitive to the iron content of H. As the relatively low iron content of HL3 provides high amount of PSMP retention (inferred from the low plateau concentration), the presence of optimal hematite content between 2.3 (HL3) and 16.1 (H) can be anticipated where 100 % retention of PSMP can be achieved without straining. The higher k_{att} and S_{max} at higher hematite content (Fig. 5(c)) also confirmed that the increase in iron content increases the attachment rate and long-term retention of PSMP. The abrupt increase in S_{max} between HL1 and HL3 and the slight increase in S_{max} between HL3 (0.928 mg/g) and H (1.207 mg/g) indicates that the long-term retention of PSMP can be achieved at low hematite content.

As previously mentioned, the attachment efficiencies of H and M shown in this study did not exhibit significant differences ($G > H > M$ or $G > H \sim M$). Previous studies have reported that M demonstrated a higher retention of PSMP compared to H. However, this discrepancy can be attributed to the higher coated mass of magnetite compared to that of hematite (e.g., 1.5 times higher iron content for magnetite than hematite (Choudhary et al., 2024)). The lower retention of HL1, HL2, and HL3 compared to M shown in this study is consistent with the previous observation, which can be attributed to the lower iron content of HL1, HL2, and HL3 than M. Further investigation would be required to investigate the retention efficiency between H and M at given iron content or potential influencing factor on the PSMP retention such as specific surface area of iron oxides (58.9 m^2/g for magnetite and 5.6 m^2/g for hematite; Choudhary et al., 2024). The lower iron content for G compared to the other iron oxides tested in this study indicates that G can be the most efficient iron oxide particle in retained mass of PSMPs per unit mass of iron oxides.

4. Discussion

Hematite, goethite, and magnetite are typically present in residual soils such as ferralsols (Nitzsche et al., 2008) and gleysols (Doum et al., 2020) and are frequently found in waste streams of mines, riverbanks, and floodplains (Geise et al., 2011; Keim et al., 2021; Quinton et al., 2011). Additionally, hematite and goethite are often found in aquifers as coatings on the surface of soil particles (Buerge-Weirich et al., 2002). Therefore, the experimental results shown in this study imply that the presence of iron oxides at the surface of natural soils can retard the transport of PSMPs where the mobility of PSMPs can vary depending on SR, iron oxide content, type of iron oxide, and IS. Although the presence of iron oxide may not always lead to the retardation of PSMP transport because of the complex chemical composition of natural soils, the results shown in this study provide an insight into the transport of PSMP under the presence of iron oxides in natural soils. The higher mass of retained PSMP for three IOCSs compared to quartz sand also implies the chance of applying IOCS in a permeable reactive barrier to remove PSMP.

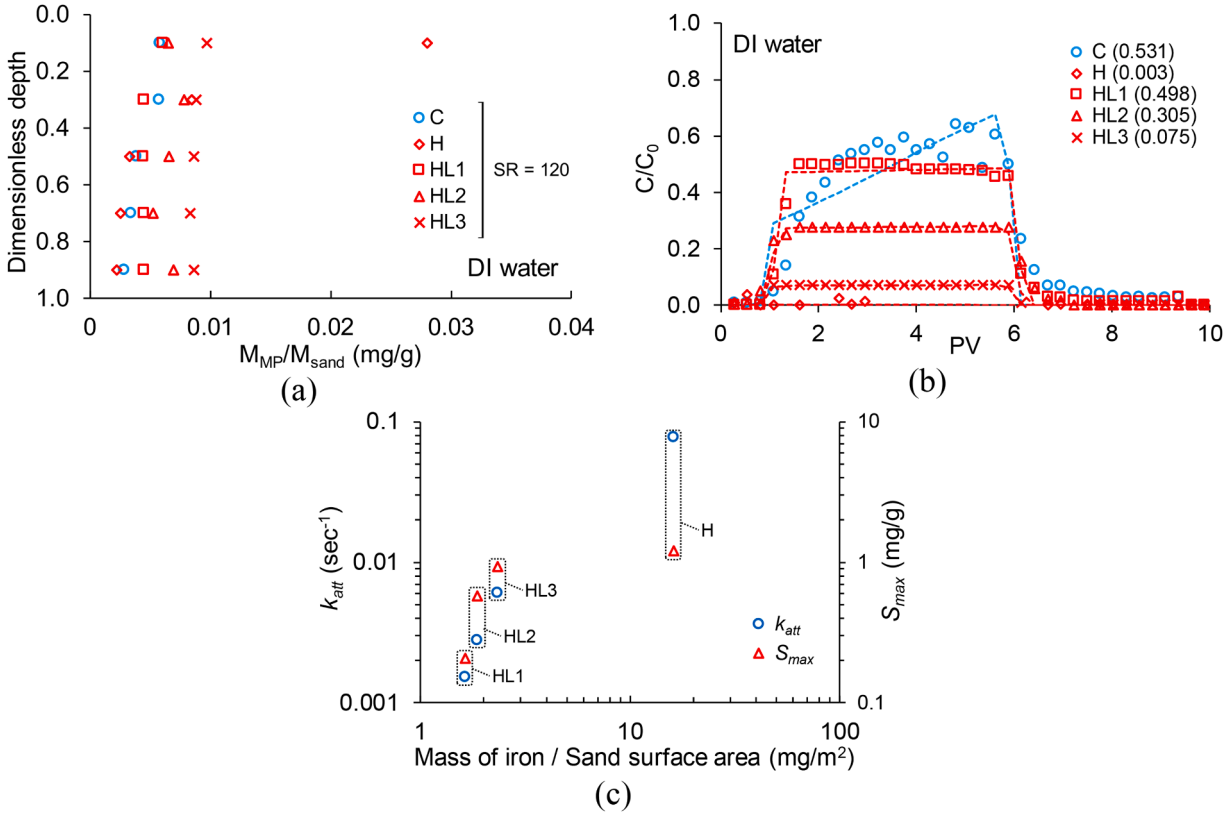

Fig. 5. Observed (a) RPs, (b) BTCs, and (c) iron content vs optimized k_{att} and S_{max} for low-content hematite IOCS (HL1, HL2, and HL3). The values for C and H are the same as those in Figs. 3(a), 4(a, c), and 6(a). The numbers in parenthesis (b) indicate the M_e (Table S3) in each case. The dotted line in (b) shows the fit results for each case.

Almost no tailing effect of PMSP was observed at pH = 4 – 9 and IS > 1 mM under SR = 1000 – 4000 of iron oxide-coated silica sand in previous studies (Chang et al., 2023; Wu et al., 2022). This is consistent with the almost no tailing effect observed in this study (Fig. 2) under SR = 120–720, implying that relatively stable attachment of PSMP on IOCS without any significant detachment can be anticipated in a wide range of SR with stable solution chemistry. In contrast, a slight tailing effect ($C/C_0 > 0.03$) was observed for clean sand under IS = 0 M for SR = 120, 550, and 720 (Figs. 2(a), 2(e), and 2(g)), indicating relatively weak attraction between clean sand and PSMP. Overall, the observed BTCs shown in this study suggest that iron-rich soils can provide not only high retention rate but also stable long-term retention of PSMP compared to soils without iron oxides.

The experimental pH = 6.9 applied in this study is close to the IEP of goethite (pH = 8), magnetite (pH = 7.5), and hematite (pH = 7) (Choudhary et al., 2024; Rusch et al., 2010). Considering that carboxyl-modified PSMP particles have an IEP below pH = 2 (Xie et al., 2023), similar retention behavior is expected within a pH range of approximately 4 to the IEPs of each iron oxide (pH 7–8) due to favorable electrostatic interactions that promote PSMP attachment to IOCS surfaces. Under extremely low pH conditions (< pH 4), IOCSs cannot be used in the experiment because dissolution of iron oxide likely occurs at low pH. At pH levels above ~8, PSMP retention is expected to be very low as both IOCS surfaces and PSMPs carry negative charges (unfavorable attachment condition) (Wu et al., 2022). However, the higher roughness of IOCSs compared to clean sand may slightly enhance PSMP retention under these conditions. Xiao et al. (2024) reported that the retention of PSMPs under vertical upward, diagonal upward, and diagonal downward flow was 3.4, 2.2, and 1.6 times higher than that under vertical downward flow (SR = 472). This implies that the retention of PSMPs observed in this study under vertical downward flow could be even higher in different flow directions. In addition, as the lower hydraulic shear stress at higher d_{50} can be anticipated (i.e., higher hydraulic conductivity at higher d_{50} (Fig. S10)), the more significant reduction of PSMP retention at SR = 720 compared to SR = 120 can be anticipated under constant head condition (i.e., identical lower hydraulic shear stress). As the naturally induced hydraulic shear stress is relatively consistent (Rosgen, 1994), the presence of iron-rich soils with low SR can be highly beneficial in facilitating retention of PSMPs in a natural subsurface environment.

In natural environments, iron oxides primarily adsorbed to soil particles in a stable state (Olivie-Lauquet et al., 2001; Schwertmann, 1991). However, iron oxides are occasionally present in pore water as colloidal particles, implying the chance of encountering PSMP in the aqueous phase, particularly under iron oxide-riched environments. Under such environments, the aggregation between PSMP and colloidal iron oxides can be anticipated (Vu et al., 2022), which can increase the retention of PSMP at low SR due to high straining effect. As the observed RPs in this study are under the absence of colloidal iron oxides in the aqueous phase (i.e., presence of iron oxides in the solid phase), further investigation can be required to investigate the impact of the presence of iron oxides in solid and aqueous phases to assess the impact of iron oxide-PSMP aggregation on retention of PSMP.

5. Conclusion

This study investigated the transport of PSMPs through saturated uncoated sand and three IOCSs (hematite-, magnetite-, and goethite-coated sand) using soil-column experiments. Based on the observed BTCs, RPs, optimized parameters, and calculated interaction energy as a function of SR, IS, and the type of iron oxides, the following conclusions can be drawn:

1) Lower BTCs of PSMP at IS = 5 mM than IS = 0 M for the clean sand and three IOCSs were observed, which suggests that the increase in IS enhances the attachment rate of PSMP in the sand medium.
2) Lower BTCs of PSMP were observed at lower SR of IOCSs, implying that the high specific surface area of IOCSs is beneficial in the retention of PSMP.
3) Almost no tailing effect of PSMP for the three IOCSs indicates the long-term stable retention of PSMP using IOCSs.
4) Goethite-coated sand showed the highest PSMP retention between the three IOCSs, particularly at IS = 0 M. The difference in PSMP retention among the three IOCSs was insignificant in all SRs at IS = 5 mM.
5) Relatively straight RPs for the rest of the experimental conditions indicate attachment-dominant retention of PSMP under SR = 120 – 720. However, the hyperexponential RP for H at SR = 120 suggests that the type of iron oxides can affect the retention behavior of PSMPs at given SR.
6) The order of energy barrier as $G < H \sim M < C$ from the interaction energy calculated by XDLVO theory was consistent with the order of PSMP retention observed in BTCs.

CRediT authorship contribution statement

Yongjoon Choe: Visualization, Investigation, Formal analysis, Data curation, Conceptualization, Writing – original draft. **Jongmuk Won:** Writing – review & editing, Validation, Supervision. **Susan E. Burns:** Writing – review & editing, Project administration, Funding acquisition.

Declaration of competing interest

The authors declare that they have no known competing financial interests or personal relationships that could have appeared to influence the work reported in this paper.

Acknowledgements

This study was supported by National Research Foundation of Korea (NRF) grants funded by the Korean government (MSIT) (RS-2023-00221719 and 2022R1C1C1007296).

Supplementary materials

Supplementary material associated with this article can be found, in the online version, at doi:10.1016/j.watres.2024.122856.

Data availability

The datasets generated during and/or analyzed during the current study are available from the corresponding author upon reasonable request.

References

Ahammed, M.M., Davra, K., 2011. Performance evaluation of biosand filter modified with iron oxide-coated sand for household treatment of drinking water. Desalination 276, 287–293. https://doi.org/10.1016/j.desal.2011.03.065.

Al Harraq, A., Bharti, B., 2022. Microplastics through the Lens of Colloid Science. ACS Environ. Au 2, 3–10. https://doi.org/10.1021/acsenvironau.1c00016.

Albinger, O., Biesemeyer, B.K., Arnold, R.G., Logan, B.E., 1994. Effect of bacterial heterogeneity on adhesion to uniform collectors by monoclonal populations. FEMS Microbiol. Lett. 124, 321–326. https://doi.org/10.1111/j.1574-6968.1994.tb07303.x.

Alimi, O.S., Claveau-Mallet, D., Kurusu, R.S., Lapointe, M., Bayen, S., Tufenkji, N., 2022. Weathering pathways and protocols for environmentally relevant microplastics and nanoplastics: what are we missing? J. Hazard. Mater. 423. https://doi.org/10.1016/j.jhazmat.2021.126955.

Andrady, A.L., 2011. Microplastics in the marine environment. Mar. Pollut. Bull. 62, 1596–1605. https://doi.org/10.1016/j.marpolbul.2011.05.030.

Auta, H.S., Emenike, C.U., Fauziah, S.H., 2017. Distribution and importance of microplastics in the marine environment: a review of the sources, fate, effects, and potential solutions. Environ. Int. 102, 165–176. https://doi.org/10.1016/j.envint.2017.02.013.

Baygents, J.C., Glynn, J.R., Albinger, O., Biesemeyer, B.K., Ogden, K.L., Arnold, R.G., 1998. Variation of surface charge density in monoclonal bacterial populations:

implications for transport through porous media. Environ. Sci. Technol. 32, 1596–1603. https://doi.org/10.1021/es9707116.
Benjamin, M.M., Sletten, R.S., Bailey, R.P., Bennett, T., 1996. Sorption and filtration of metals using iron-oxide-coated sand. Water Res 30, 2609–2620. https://doi.org/10.1016/S0043-1354(96)00161-3.
Blaga, A., 1980. Deterioration mechanisms in weathering of plastic materials. Durab. Build. Mater. Components 827–837. https://doi.org/10.1520/STP36112S.
Blakey, B.C., James, D.F., 2003. The viscous behaviour and structure of aqueous suspensions of goethite. Colloids Surf. A Physicochem. Eng. Asp. 231, 19–30. https://doi.org/10.1016/j.colsurfa.2003.08.019.
Boots, B., Russell, C.W., Green, D.S., 2019. Effects of microplastics in soil ecosystems: above and below ground. Environ. Sci. Technol. 53, 11496–11506. https://doi.org/10.1021/acs.est.9b03304.
Bradford, S.A., Kim, H., Shen, C., Sasidharan, S., Shang, J., 2017. Contributions of nanoscale roughness to anomalous colloid retention and stability behavior. Langmuir 33, 10094–10105. https://doi.org/10.1021/acs.langmuir.7b02445.
Bradford, S.A., Simunek, J., Bettahar, M., Tadassa, Y.F., van Genuchten, M.T., Yates, S.R., 2005. Straining of colloids at textural interfaces. Water Resour. Res. 41. https://doi.org/10.1029/2004WR003675.
Bradford, S.A., Simunek, J., Bettahar, M., van Genuchten, M.T., Yates, S.R., 2003. Modeling colloid attachment, straining, and exclusion in saturated porous media. Environ. Sci. Technol. 37, 2242–2250. https://doi.org/10.1021/es025899u.
Bradford, S.A., Torkzaban, S., Simunek, J., 2011. Modeling colloid transport and retention in saturated porous media under unfavorable attachment conditions. Water Resour. Res. 47. https://doi.org/10.1029/2011WR010812.
Brewer, A., Dror, I., Berkowitz, B., 2020. The mobility of plastic nanoparticles in aqueous and soil environments: a critical review. Environ. Sci. Technol. Water 1, 48–57. https://doi.org/10.1021/acsestwater.0c00130.
Buerge-Weirich, D., Hari, R., Xue, H., Behra, P., Sigg, L., 2002. Adsorption of Cu, Cd, and Ni on goethite in the presence of natural groundwater ligands. Environ. Sci. Technol. 36, 328–336. https://doi.org/10.1021/es010892i.
Büks, F., Kaupenjohann, M., 2022. What comes after the Sun? On the integration of soil biogeochemical pre-weathering into microplastic experiments. Soil 8, 373–380. https://doi.org/10.5194/soil-8-373-2022.
Cai, L., Peng, S., Wu, D., Tong, M., 2016. Effect of different-sized colloids on the transport and deposition of titanium dioxide nanoparticles in quartz sand. Environ. Pollut. 208, 637–644. https://doi.org/10.1016/j.envpol.2015.10.040.
Carpenter, E.J., Anderson, S.J., Harvey, G.R., Miklas, H.P., Peck, B.B., 1972. Polystyrene spherules in coastal waters. Science 178, 749–750. https://doi.org/10.1126/science.178.4062.750.
Chang, B., He, B., Cao, G., Zhou, Z., Liu, X., Yang, Y., Xu, C., Hu, F., Lv, J., Du, W., 2023. Co-transport of polystyrene microplastics and kaolinite colloids in goethite-coated quartz sand: joint effects of heteropolymerization and surface charge modification. Sci. Total Environ. 884, 163832. https://doi.org/10.1016/j.scitotenv.2023.163832.
Chen, J., Lu, T., Wang, Y., Li, J., Fu, X., Qi, Z., Zhang, Q., 2019. Transport of graphene oxide nanoparticles in saturated kaolinite-and goethite-coated sand columns: effects of low-molecular-weight organic acids. Environ. Sci. Pollut. Res. 26, 24922–24932. https://doi.org/10.1007/s11356-019-05683-0.
Choe, Y., Choi, H., Won, J., 2022. Suffusion of a sand-clay mixture: impact of the ionic-concentration gradient, clay type, sand-grain size, and hydraulic gradient. Geotechnique. https://doi.org/10.1680/jgeot.21.00335.
Choudhary, A., Khandelwal, N., Ganie, Z.A., Darbha, G.K., 2024. Influence of magnetite and its weathering originated maghemite and hematite minerals on sedimentation and transport of nanoplastics in the aqueous and subsurface environments. Sci. Total Environ. 912. https://doi.org/10.1016/j.scitotenv.2023.169132.
Cooper, D.A., 2012. Effects of Chemical and Mechanical Weathering Processes On the Degradation of Plastic Debris On Marine Beaches. The University of Western Ontario.
Corcoran, P.L., 2022. Degradation of microplastics in the environment. Handb. Microplastics Environ. 531–542. https://doi.org/10.1007/978-3-030-39041-9_10.
Cuddy, M.F., Poda, A.R., Brantley, L.N., 2013. Determination of Isoelectric Points and the Role of pH for Common Quartz Crystal Microbalance Sensors. ACS Appl. Mater. Interfaces 5, 3514–3518. https://doi.org/10.1021/am400909g.
Deng, Y., Zhang, Y., Lemos, B., Ren, H., 2017. Tissue accumulation of microplastics in mice and biomarker responses suggest widespread health risks of exposure. Sci. Rep. 7, 1–10. https://doi.org/10.1038/srep46687.
Dong, P., Liang, Y., Shen, C., Jiang, E., Bradford, S.A., 2024. Dual roles of goethite coating on the transport of plastic nanoparticles in heterogeneous porous media: the significance of collector surface roughness. J. Hazard. Mater. 470, 134153. https://doi.org/10.1016/j.jhazmat.2024.134153.
Doum, J.M., Fuh, G.C., Fadil-Djenabou, S., Onana, V.L., Ndjigui, P.D., Armstrong-Altrin, J.S., 2020. Characterization and potential application of gleysols and ferralsols for ceramic industry: a case study from Dimako (Eastern Cameroon). Arab. J. Geosci. 13, 1–22. https://doi.org/10.1007/s12517-020-06007-0.
Duan, J., Bolan, N., Li, Y., Ding, S., Atugoda, T., Vithanage, M., Sarkar, B., Tsang, D.C.W., Kirkham, M.B., 2021. Weathering of microplastics and interaction with other coexisting constituents in terrestrial and aquatic environments. Water Res 196, 117011. https://doi.org/10.1016/j.watres.2021.117011.
Ebere, E.C., Wirnkor, V.A., Ngozi, V.E., 2019. Uptake of microplastics by plant: a reason to worry or to be happy? World Sci. News 131, 256–267.
Faure, B., Salazar-Alvarez, G., Bergstrom, L., 2011. Hamaker constants of iron oxide nanoparticles. Langmuir 27, 8659–8664. https://doi.org/10.1021/la201387d.
Flury, M., Czigány, S., Chen, G., Harsh, J.B., 2004. Cesium migration in saturated silica sand and Hanford sediments as impacted by ionic strength. J. Contam. Hydrol. 71, 111–126. https://doi.org/10.1016/j.jconhyd.2003.09.005.
Fotopoulou, K.N., Karapanagioti, H.K., 2012. Surface properties of beached plastic pellets. Mar. Environ. Res. 81, 70–77. https://doi.org/10.1016/j.marenvres.2012.08.010.
Geise, G., LeGalley, E., Krekeler, M.P.S., 2011. Mineralogical and geochemical investigations of silicate-rich mine waste from a kyanite mine in central Virginia: implications for mine waste recycling. Environ. Earth Sci. 62, 185–196. https://doi.org/10.1007/s12665-010-0513-7.
Geyer, R., Jambeck, J.R., Law, K.L., 2017. Production, use, and fate of all plastics ever made. Sci. Adv. 3, 25–29. https://doi.org/10.1126/sciadv.1700782.
Hanna, K., 2007. Adsorption of aromatic carboxylate compounds on the surface of synthesized iron oxide-coated sands. Appl. Geochem. 22, 2045–2053. https://doi.org/10.1016/j.apgeochem.2007.05.005.
Hitchcock, J.N., 2020. Storm events as key moments of microplastic contamination in aquatic ecosystems. Sci. Total Environ. 734. https://doi.org/10.1016/j.scitotenv.2020.139436.
Hoggan, J.L., Sabatini, D.A., Kibbey, T.C.G., 2016. Transport and retention of TiO2 and polystyrene nanoparticles during drainage from tall heterogeneous layered columns. J. Contam. Hydrol. 194, 30–35. https://doi.org/10.1016/j.jconhyd.2016.10.003.
Horton, A.A., Dixon, S.J., 2018. Microplastics: an introduction to environmental transport processes. Wiley Interdiscip. Rev. Water 5. https://doi.org/10.1002/WAT2.1268.
Hwang, J., Choi, D., Han, S., Jung, S.Y., Choi, J., Hong, J., 2020. Potential toxicity of polystyrene microplastic particles. Sci. Rep. 10, 1–12. https://doi.org/10.1038/s41598-020-64464-9.
Jeong, B., Kim, J.S., Kwon, A.R., Lee, J., Park, S., Koo, J., Lee, W.S., Baek, J.Y., Shin, W. H., Lee, J.S., Jeong, J., Kim, W.K., Jung, C.R., Kim, N.S., Cho, S.H., Lee, D.Y., 2024. Maternal nanoplastic ingestion induces an increase in offspring body weight through altered lipid species and microbiota. Environ. Int. 185. https://doi.org/10.1016/j.envint.2024.108522.
Joshi, A., Chaudhuri, M., 1996. Removal of arsenic from ground water by iron oxide-coated sand. J. Environ. Eng. 122, 769–771. https://doi.org/10.1061/(asce)0733-9372(1996)122:8(769).
Karbalaei, S., Hanachi, P., Walker, T.R., Cole, M., 2018. Occurrence, sources, human health impacts and mitigation of microplastic pollution. Environ. Sci. Pollut. Res. 25, 36046–36063. https://doi.org/10.1007/s11356-018-3508-7.
Keim, C.N., Serna, J.D.P., Acosta-Avalos, D., Neumann, R., Silva, A.S., Jurelevicius, D.A., Pereira, R.S., de Souza, P.M., Seldin, L., Farina, M., 2021. Dissimilatory Iron-reducing microorganisms are present and active in the sediments of the Doce River and tributaries impacted by Iron mine tailings from the collapsed Fundão dam (Mariana, MG, Brazil). Minerals 11 244. https://doi.org/10.3390/min11030244.
Kibria, M.G., Masuk, N.I., Safayet, R., Nguyen, H.Q., Mourshed, M., 2023. Plastic waste: challenges and opportunities to mitigate pollution and effective management. Int. J. Environ. Res. https://doi.org/10.1007/s41742-023-00507-z.
Lai, C., Lo, S., Lin, C., 1994. Mechanisms of iron oxide coating onto sand surface and its adsorption behaviors for copper. Toxicol. Environ. Chem. 46, 107–118. https://doi.org/10.1080/02772249409358103.
Larrahondo, J.M., Burns, S.E., 2014. Laboratory-prepared iron oxide coatings on sands: surface characterization and strength parameters. J. Geotech. Geoenvironmental. Eng. 140, 1–9. https://doi.org/10.1061/(asce)gt.1943-5606.0001068.
Larrahondo, J.M., Choo, H., Burns, S.E., 2011. Laboratory-prepared iron oxide coatings on sands: submicron-scale small-strain stiffness. Eng. Geol. 121, 7–17. https://doi.org/10.1016/j.enggeo.2011.04.009.
Li, J., Song, Y., Cai, Y., 2020. Focus topics on microplastics in soil: analytical methods, occurrence, transport, and ecological risks. Environ. Pollut. 257. https://doi.org/10.1016/j.envpol.2019.113570.
Li, X., Scheibe, T.D., Johnson, W.P., 2004. Apparent decreases in colloid deposition rate coefficients with distance of transport under unfavorable deposition conditions: a general phenomenon. Environ. Sci. Technol. 38, 5616–5625. https://doi.org/10.1021/es049154v.
Liu, P., Zhan, X., Wu, X., Li, J., Wang, H., Gao, S., 2020. Effect of weathering on environmental behavior of microplastics: properties, sorption and potential risks. Chemosphere 242. https://doi.org/10.1016/j.chemosphere.2019.125193.
Magal, E., Weisbrod, N., Yechieli, Y., Walker, S.L., Yakirevich, A., 2011. Colloid transport in porous media: impact of hyper-saline solutions. Water Res. 45, 3521–3532. https://doi.org/10.1016/j.watres.2011.04.021.
Mitropoulou, P.N., Syngouna, V.I., Chrysikopoulos, C.V., 2013. Transport of colloids in unsaturated packed columns: role of ionic strength and sand grain size. Chem. Eng. J. 232, 237–248. https://doi.org/10.1016/j.cej.2013.07.093.
Nitzsche, R.P., Percival, J.B., Torrance, J.K., Stirling, J.A.R., Bowen, J.T., 2008. X-ray diffraction and infrared characterization of Oxisols from central and southeastern Brazil. Clay Miner 43, 549–560. https://doi.org/10.1180/claymin.2008.043.4.03.
Olivie-Lauquet, G., Gruau, G., Dia, A., Riou, C., Jaffrezic, A., Henin, O., 2001. Release of trace elements in wetlands: role of seasonal variability. Water Res 35, 943–952. https://doi.org/10.1016/S0043-1354(00)00328-6.
Peng, S., Wu, D., Ge, Z., Tong, M., Kim, H., 2017. Influence of graphene oxide on the transport and deposition behaviors of colloids in saturated porous media. Environ. Pollut. 225, 141–149. https://doi.org/10.1016/j.envpol.2017.03.064.
Quinton, E.E., Dahms, D.E., Geiss, C.E., 2011. Magnetic analyses of soils from the Wind River Range, Wyoming, constrain rates and pathways of magnetic enhancement for soils from semiarid climates. Geochem. Geophys. Geosystems 12. https://doi.org/10.1029/2011GC003728.
Redman, J.A., Grant, S.B., Olson, T.M., Estes, M.K., 2001. Pathogen filtration, heterogeneity, and the potable reuse of wastewater. Environ. Sci. Technol. 35, 1798–1805. https://doi.org/10.1021/es0010960.

Ren, D., Smith, J.A., 2013. Proteinate-capped silver nanoparticle transport in water-saturated sand. J. Environ. Eng. 139, 781–787. https://doi.org/10.1061/(asce)ee.1943-7870.0000684.
Ritchie, H., Samborska, V., Roser, M., 2023. Plastic Pollution. Our World Data.
Rosgen, D.L., 1994. A classification of natural rivers. Catena 22, 169–199. https://doi.org/10.1016/0341-8162(94)90001-9.
Rusch, B., Hanna, K., Humbert, B., 2010. Coating of quartz silica with iron oxides: characterization and surface reactivity of iron coating phases. Colloids Surfaces A Physicochem. Eng. Asp. 353, 172–180. https://doi.org/10.1016/j.colsurfa.2009.11.009.
Saberinasr, A., Rezaei, M., Nakhaei, M., Hosseini, S.M., 2016. Transport of CMC-Stabilized nZVI in saturated sand column: the effect of particle concentration and soil grain size. Water, Air, Soil Pollut 227, 1–16. https://doi.org/10.1007/s11270-016-3097-3.
Schwertmann, U., 1991. Solubility and dissolution of iron oxides. Plant Soil 130, 1–25. https://doi.org/10.1007/BF00011851.
Selvam, S., Jesuraja, K., Venkatramanan, S., Roy, P.D., Jeyanthi Kumari, V., 2021. Hazardous microplastic characteristics and its role as a vector of heavy metal in groundwater and surface water of coastal south India. J. Hazard. Mater. 402, 123786. https://doi.org/10.1016/j.jhazmat.2020.123786.
Shen, C., Li, B., Huang, Y., Jin, Y., 2007. Kinetics of coupled primary-and secondary-minimum deposition of colloids under unfavorable chemical conditions. Environ. Sci. Technol. 41, 6976–6982. https://doi.org/10.1021/es070210c.
Shruti, V.C., Pérez-Guevara, F., Elizalde-Martínez, I., Kutralam-Muniasamy, G., 2021. Current trends and analytical methods for evaluation of microplastics in stormwater. Trends Environ. Anal. Chem. 30. https://doi.org/10.1016/j.teac.2021.e00123.
Song, Y.K., Hong, S.H., Jang, M., Han, G.M., Jung, S.W., Shim, W.J., 2017. Combined effects of UV exposure duration and mechanical abrasion on microplastic fragmentation by polymer type. Environ. Sci. Technol. 51, 4368–4376. https://doi.org/10.1021/acs.est.6b06155.
Stahl, R.S., James, B.R., 1991. Zinc sorption by iron-oxide-coated sand as a function of pH. Soil Sci. Soc. Am. J. 55, 1287–1290. https://doi.org/10.2136/sssaj1991.03615995005500050015x.
Thirunavukkarasu, O.S., Viraraghavan, T., Subramanian, K.S., 2003. Arsenic removal from drinking water using iron oxide-coated sand. Water, Air, Soil Pollut 142, 95–111. https://doi.org/10.1023/A:1022073721853.
Torkzaban, S., Bradford, S.A., van Genuchten, M.T., Walker, S.L., 2008. Colloid transport in unsaturated porous media: the role of water content and ionic strength on particle straining. J. Contam. Hydrol. 96, 113–127. https://doi.org/10.1016/j.jconhyd.2007.10.006.
Vu, T.T.T., Nguyen, P.H., Pham, T.V., Do, P.Q., Dao, T.T., Nguyen, A.D., Nguyen-Thanh, L., Dinh, V.M., Nguyen, M.N., 2022. Comparative effects of crystalline, poorly crystalline and freshly formed iron oxides on the colloidal properties of polystyrene microplastics. Environ. Pollut. 306, 119474. https://doi.org/10.1016/j.envpol.2022.119474.
Wang, D., Ge, L., He, J., Zhang, W., Jaisi, D.P., Zhou, D., 2014. Hyperexponential and nonmonotonic retention of polyvinylpyrrolidone-coated silver nanoparticles in an Ultisol. J. Contam. Hydrol. 164, 35–48. https://doi.org/10.1016/j.jconhyd.2014.05.007.
Wang, L., Wu, W.M., Bolan, N.S., Tsang, D.C.W., Li, Y., Qin, M., Hou, D., 2021. Environmental fate, toxicity and risk management strategies of nanoplastics in the environment: current status and future perspectives. J. Hazard. Mater. 401, 123415. https://doi.org/10.1016/j.jhazmat.2020.123415.
Wikiniyadhanee, R., Chotpantarat, S., Ong, S.K., 2016. Kaolinite and Cd 2+ transport and interaction in sand media: batch and column experiments. Terr. Atmos. Ocean. Sci. 27. https://doi.org/10.3319/TAO.2015.10.26.01(TT).
Won, J., Burns, S.E., 2022. Role of ionic concentration in the kinetic attachment of kaolinite and sand. Can. Geotech. J. https://doi.org/10.1139/CGJ-2021-0682.
Won, J., Choe, Y., Yang, Y., Choi, H., 2023. Impact of clay particle reattachment on suffusion of sand–clay mixtures. J. Rock Mech. Geotech. Eng. https://doi.org/10.1016/j.jrmge.2022.12.013.
Won, J., Choo, H., Burns, S.E., 2020. Impact of solution chemistry on deposition and breakthrough behaviors of kaolinite in silica sand. J. Geotech. Geoenvironmental Eng. 146. https://doi.org/10.1061/(ASCE)GT.1943-5606.0002199.
Wu, X., Zeng, X., Lyu, X., Gao, B., Sun, Y., Wu, J., 2022. Combined effects of Fe/Al oxyhydroxide coating and pH on polystyrene nanoplastic transport in saturated sand media. Water, Air, Soil Pollut 233 (2). https://doi.org/10.1007/s11270-021-05469-6.
Xiao, D., Li, S., Chen, Z., Zou, S., Nugroho, W.A., Huo, M., Fan, W., 2024. Microplastic and silica colloid transport in a saturated porous medium under various flow directions: the effect of gravity. Water Air Soil Pollut 235, 3. https://doi.org/10.1007/s11270-023-06824-5.
Xie, R., Xing, X., Nie, X., Ma, X., Wan, Q., Chen, Q., Li, Z., Wang, J., 2023. Deposition behaviors of carboxyl-modified polystyrene nanoplastics with goethite in aquatic environment: effects of solution chemistry and organic macromolecules. Sci. Total Environ. 904, 166783. https://doi.org/10.1016/j.scitotenv.2023.166783.
Xu, S., Gao, B., Saiers, J.E., 2006. Straining of colloidal particles in saturated porous media. Water Resour. Res. 42, 12. https://doi.org/10.1029/2006WR004948.
Yoshida, T., Suzuki, M., 2006. Migration of strontium and europium in quartz sand column in the presence of humic acid: effect of ionic strength. J. Radioanal. Nucl. Chem. 270, 363–368. https://doi.org/10.1007/s10967-006-0358-4.